Mechanical basis for slip along low-angle normal faults

Emmanuel Lecomte,[1] Laetitia Le Pourhiet,[2,3] and Olivier Lacombe[2,3]

[1] The existence of active low-angle normal faults is much debated because (1) the classical theory of fault mechanics implies that normal faults are locked when the dip is less than 30° and (2) shallow-dipping extensional fault planes do not produce large earthquakes (M > 5.5). However, a number of field observations suggest that brittle deformation occurs on low-angle normal faults at very shallow dip. To reconcile observations and theory, we use an alternative model of fault reactivation including a thick elasto-plastic frictional fault gouge, and test it at large strain by the mean of 2D mechanical modeling. We show that plastic compaction allows reducing the effective friction of faults sufficiently for low-angle normal faults to be active at dip of 20°. As the model predicts that these faults must be active in a slip-hardening regime, it prevents the occurrence of large earthquakes. However, we also evidence the neoformation of Riedel-type shear bands within thick fault zone, which, we believe, may be responsible for repeated small earthquakes and we apply the model to the Gulf of Corinth (Greece). **Citation:** Lecomte, E., L. Le Pourhiet, and O. Lacombe (2012), Mechanical basis for slip along low-angle normal faults, *Geophys. Res. Lett.*, *39*, L03307, doi:10.1029/2011GL050756.

1. Introduction

[2] Despite the lack of *M* > 5.5 earthquakes on low-angle normal faults (LANF) [*Jackson and White*, 1989; *Collettini and Sibson*, 2001], micro-seismic activity is found to occur along shallow-dipping fault planes in the Western Gulf of Corinth [*Rigo et al.*, 1996] or in the Apennines [*Chiaraluce et al.*, 2007]. The presence of brecciated gouges and cataclasites around and within exhumed LANF advocates for a brittle frictional behavior of these fault zones [*Lister and Davis*, 1989; *Hayman et al.*, 2003; *Collettini and Holdsworth*, 2004; *Lecomte et al.*, 2010]. The common occurrence of vertical mode I cracks or veins associated with the deformation on exhumed LANFs implies that the maximum principal stress σ_1 was sub-vertical [e.g., *Mehl et al.*, 2005, 2007], while the geometry of the syn-extension sedimentary deposits supports that the LANFs did not rotate significantly [e.g., *Lecomte et al.*, 2010]. Under a sub-vertical maximum principal stress, slip along a LANF dipping 20° in drained condition requires the friction of the fault to be as low as 0.2 (or up to 0.36 for fluid overpressure), which leads to usually classify LANFs as weak faults.

[3] This extreme weakness can partly be explained by high pore fluid pressure [*Collettini and Sibson*, 2001], by the presence of phyllosilicates in the gouge [*Numelin et al.*, 2007; *Haines et al.*, 2009], or a combined effect of the two. However, in extensional setting, the fluid pressure cannot exceed the minimum horizontal stress [*Sibson*, 1990] and the friction of rocks must still be as low as 0.36 [*Collettini and Sibson*, 2001]. Similarly, the widespread development of phyllosilicates is not a so common feature for most of the exhumed LANF [see *Collettini*, 2011, and references therein]. While these two processes contribute to lower the effective friction of mature natural fault zones as compared to the surrounding rocks, the effect related to secondary micro-structures and to the evolution of the thickness of the fault in response to slip on these micro-structures starts only to be explored in theory [*Lecomte et al.*, 2011] and in the laboratory [*Ikari et al.*, 2011].

[4] Although rocks are often regarded as dilatant material, numbers of field observations suggest that mature fault zones compact with shear. The presence of S-C or C′ foliation within fault zone [e.g., *Collettini*, 2011] is a kinematic argument for the flattening of the shear zone [*Platt and Vissers*, 1980]. The wavelength of the mullions in fault zones can be fitted with analytical solution for the dynamic growth of mullions and boudins [*Sagy and Brodsky*, 2009] which therefore provides a dynamic support for fault flattening with shear. In the laboratory, the transition from dilating to compacting shear bands is observed to occur with increasing confining pressure in clay [*Roscoe et al.*, 1958] and in sandstones [*Bésuelle et al.*, 2000; *Mair et al.*, 2002).

[5] Based on deformation of a synthetic rock material made of salt and phyllosilicates, *Niemeijer et al.* [2009] also pointed out that grain size reduction and significant compaction (thinning) of the gouge occur together with slip softening. This behavior is well captured by the thick fault model described in details by *Lecomte et al.* [2011]. In this contribution, we first summarize the thick fault model theory, before testing its prediction at large strain by means of 2D mechanical models and finally by comparing the results with seismological data.

## 2. Thick Fault (Fault Zone) Model

[6] The thick fault (fault zone) model considers that a fault is a thick planar structure, in which both elastic and plastic deformation occur, embedded in an elastic material. The plastic strain within the fault is computed so that the state of stress within the fault does not exceed the yield criterion. In these conditions, the direction of the plastic flow within the fault is not necessary parallel to the total displacement across the fault. This difference causes elastic strain to occur within the fault and results in a rotation of the principal stresses with shear.

[7] As the orientation of stresses evolves with strain, the effective friction is modified. The stress rotation ends when the direction of the principal stresses within the fault causes

---

[1]Institute of Petroleum Engineering, Heriot-Watt University, Edinburgh, UK.
[2]ISTEP, UMR 7193, UPMC, Université Paris 6, Paris, France.
[3]CNRS, UMR 7193, ISTEP, Paris, France.
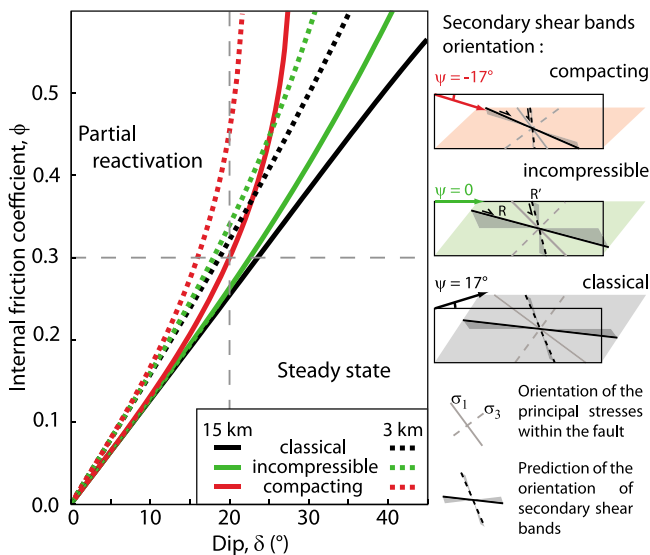
Figure 1. Locking friction coefficient as a function of the dip of low-angle normal faults for the three end-member models assuming cohesion of 10 MPa. Three sketches describe for each end-member case the total deformation of the thick fault, the predicted state of stress within the fault zone and the conjugate secondary shears consistent with these stress orientations.

the plastic flow to be parallel with the total displacement across the fault. From that stage onward, the effective friction reaches a steady state. When the fault initially makes an angle smaller than 45° with the maximum principal stress, the effective friction drops with shear strain and may lead to slip instability. However, in the case of a LANF, the fault initially makes an angle larger than 45° with the maximum principal stress, which results in an increase of the effective friction with shear strain. Within this formulation, it is possible to consider that the fault may keep a constant thickness (incompressible), thicken (dilate) or thin (compact) with shear. This component of displacement across the fault is accounted for by the dilation angle ψ, which measures the ratio of the strain normal to the fault to the total shear strain. At the end of the rotation, the orientation of the stress within, and relative to, the fault zone depends only on the value of the dilation angle ψ of the fault zone and does not depend on its dip. Given that state of stress and the internal friction ϕ, it is therefore possible to deduce the orientation of the secondary shear structures that can develop within the deforming thick fault. We summarize here the predictions of the model for three end-members (Figure 1).

[8] For an extremely dilatant fault zone ($\phi = \psi$), the effective friction is equal to the internal friction coefficient ($\mu_{eff} = \tan \phi$). The model predicts exactly the same locking angle as the classical theory of reactivation. The orientation of the secondary shears displayed on Figure 1 (black case) corresponds to X and Y shears. For a fault zone which thickness does not change with shear ($\psi = 0$), the maximum principal stress makes an angle of 45° with the fault zone, the effective friction of the thick fault drops to $\mu_{eff} = \sin \phi < \tan \phi$, corresponding to an effective friction coefficient of 0.64 for an internal friction of 0.85. The secondary shears correspond to the orientation of conjugate Riedel shears R and R' (Figure 1, green case) as already shown by *Byerlee and*

Savage [1992] to explain the weakness of the San Andreas Fault. Finally, in the case of an extremely thinning fault ($\psi = -\phi$), the maximum principal stress makes an angle of $45 - \psi/2$ with the fault. In this case, the effective friction drops to $\mu_{eff} = (\sin\phi \, \cos\psi)/(1-\sin\phi \, \sin\psi)$ and the secondary shears dip at an angle higher than that of typical Riedel shears and some of them can even dip in the direction opposite to that of the main shear zone. The secondary shear structures reflect the rate of volume change at the moment they form. In nature, it is possible that the rate of volume change evolves with shear so that different orientation of structures could be observed in the same gouge. Moreover, according to *Vermeer* [1990], the shear bands may newly form with an angle between $\pi/4 + \psi/2$ and $\pi/4 + \phi/2$ from the minimal principal stress direction within the shear band allowing several shear orientations to develop at the same time within the band. They are outlined in gray in Figure 1.

[9] The analytical solution derived in the thick fault model only characterizes the slip at one point in space on the inherited fault before a new high-angle normal fault forms. It does not allow assessing whether slip along the inherited fault zone may be coeval with slip along the high-angle normal fault. Moreover, the assumptions used to develop this semi-analytical solution are far from being geologically realistic because the stress is not allowed to rotate in the vicinity of the inherited fault and because the fault itself does not rotate as large strain occurs. It is therefore difficult to quantify whether the softening induced by stress rotation within the fault zone maybe significant at large strain (i.e., cumulated slip events) or not. In order to circumvent these limitations, we performed 2D numerical experiments using geologically relevant boundary conditions.

3. Setup of 2D Mechanical Models

[10] The models are obtained by solving the conservation of momentum equation in a pseudo-static formulation with the explicit time marching numerical code Flamar [*Yamato et al.*, 2007]. This code is generally used in the field of geodynamics where Mohr-Coulomb elasto-plastic flow rule is used routinely to model the formation of new faults and plate boundaries [*Poliakov et al.*, 1993; *Gerbault et al.*, 1999]. This rheology is mesh size dependent because it does not provide a theoretical length-scale but experience shows that newly formed shear bands correspond in general to 2–3 mesh elements in thickness with that code [*Poliakov et al.*, 1993]. In the present study, we focused on the reactivation of a thick mature natural fault and on the interaction this fault may have with surrounding faults of similar or slightly smaller length-scale. To that purpose, we have set the resolution of the mesh to be of the order of 4–5 elements within the inherited thick fault which itself imposes a length-scale for plasticity to occur in the model.

[11] The initial geometry of the model is composed of two 15 km-thick layers characterizing the brittle upper crust and the ductile lower crust (Figure 2). The thick fault is introduced as a 1 km-thick mechanical heterogeneity cutting through the upper crust and dipping 20°. The dip of 20° was chosen for its geological relevance. The model is stretched by 5 km at a constant horizontal velocity of 5 mm.yr^{-1} applied on the both lateral sides. The upper surface is a free surface with $\tau = \sigma_n = 0$, while the base of the model is a free slip boundary ($\sigma = 0$ and Vy = 0). We assume that the lower crust
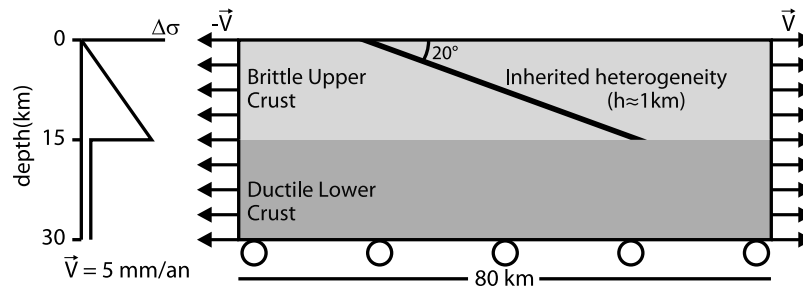
Figure 2. Setup of the 2D mechanical models.

is sufficiently weak for the Moho not to deform in response to slip along the normal fault zone, as it is the case in most of the provinces where LANFs are observed [*Allmendinger et al.*, 1987; *Makris and Vees*, 1977; *Tirel et al.*, 2004].

[12] The upper crust and the fault gouge are both characterized by a non-associated elasto-plastic Mohr-Coulomb rheology while the lower crust follows a visco-elastic rheology. The mechanical parameters for these three specific units are listed in Table 1. Frictional properties (dilation angle ψ and friction angle ϕ) of the fault gouge are listed in Table 2 since they are specific for each of the numerical experiments presented here. With internal friction of 0.3 and 0.4 and a dip of 20°, all the low-angle normal faults modeled here are close to their locking angle according to the classical reactivation theory. This suggests that the amount of strain which can be cumulated along these fault zones is low and that the fault cannot be reactivated at large strain.

4. Thick Fault Reactivation at Large Strain

[13] For all models, we computed analytically the amount of plastic strain prior to locking as a function of depth (Figure 3). With an internal friction of 0.3 and a dilation angle of 10° (Figure 3a), the analytical solution predicts the complete reactivation down to depth of 5 km and less than 1% of plastic strain before locking at greater depth. The 2D model matches the depth of the predicted complete reactivation and at deeper depth, the fault is only slightly reactivated (light blue shades) but newly-formed high-angle normal faults predominate and accommodate the extension. For the same internal friction, the model with an incompressible fault behavior (Figure 3b) also matches the limit between complete and partial reactivation obtained from the analytical solution. However, the inherited fault zone is also accommodating a large amount (>40%) of plastic strain at depth. In the compacting fault model ($\psi = -10°$, Figure 3c), the inherited fault accommodates almost all the deformation as predicted by the analytical solution. Interestingly, in the case of partial reactivation (Figures 3a, 3b, and 3d), the

reactivation of the heterogeneity seems to occur by portions, associated with the formation of a high-angle normal fault. Part of the regional extension is thus accommodated by slip along the shallow-dipping inherited fault zone. However, the amount of plastic strain cumulated along it is not sufficient to entirely accommodate the regional extension implying the formation of high-angle normal faults in the surroundings.

[14] Summarizing, our numerical models clearly show that extensional deformation can be accommodated along a shallow-dipping fault zone (dipping 20°) with internal friction of 0.3–0.4 when the fault zone is allowed to flatten with strain (negative dilation angle). This result definitely confirms that fault zone compaction is a valid mechanism for fault weakening even at large strain. The 2D models self-consistently produce a partially reactivated LANF which activity is coeval with that of high-angle normal faults. This demonstrates that LANFs and high-angle normal faults are not mutually exclusive and that the thick fault reactivation model is capable of capturing this behavior within a very raw semi-analytic solution.

5. Implication for the Seismic Hazard

[15] In the thick fault model, the reactivation of a shallow-dipping heterogeneity always occurs in a slip-hardening regime preventing dynamic slip instabilities, i.e. earthquakes, to self-nucleate [*Lecomte et al.*, 2011]. However, in the 2D models, the high-angle normal faults and the secondary shear structures within the LANF all form in a slip-weakening regime because it is a necessary condition for their localization within the adopted mechanical model [*Vermeer*, 1990]. As a result, these structures can potentially slip in the instable regime and generate earthquakes.

[16] Within the fault zone the orientation of the principal stresses is controlled by the dip and the rheological properties of the LANF. Hence, as long as we consider time scales that are sufficiently short for the LANF not to rotate significantly, the principal stress orientations remain constant in time. The secondary shear structures that develop with the LANF must therefore have a constant dip. The 2D models performed in this study have a sufficiently large resolution to allow the

Table 1. Lithological Rheological Parameters[a]

	ρ (kg.m^{-3})	η (Pa.s)	G (GPa)	ν	Co (MPa)	μ	ψ (deg)
Fault zone	2700		30	0.25	0	*var.*	*var.*
Upper Crust	2700		30	0.25	10	0.6	0
Lower Crust	2700	10^{21}	30	0.25			

[a]Parameters: ρ = density (kg.m^{-3}); η = viscosity (Pa.s); G = shear modulus (GPa); ν = Poisson's coefficient; Co = cohesion (MPa); μ = friction coefficient; ψ = dilation angle (°); *var* = variable.

Table 2. Physical Parameters Used for Each Experiment

| Model	μ	ψ (deg)	Reactivation
COMP03	0.3	−10	Complete
COMP04	0.4	−10	Partial
DILAT	0.3	10	Partial
INCOMP	0.3	0	Partial
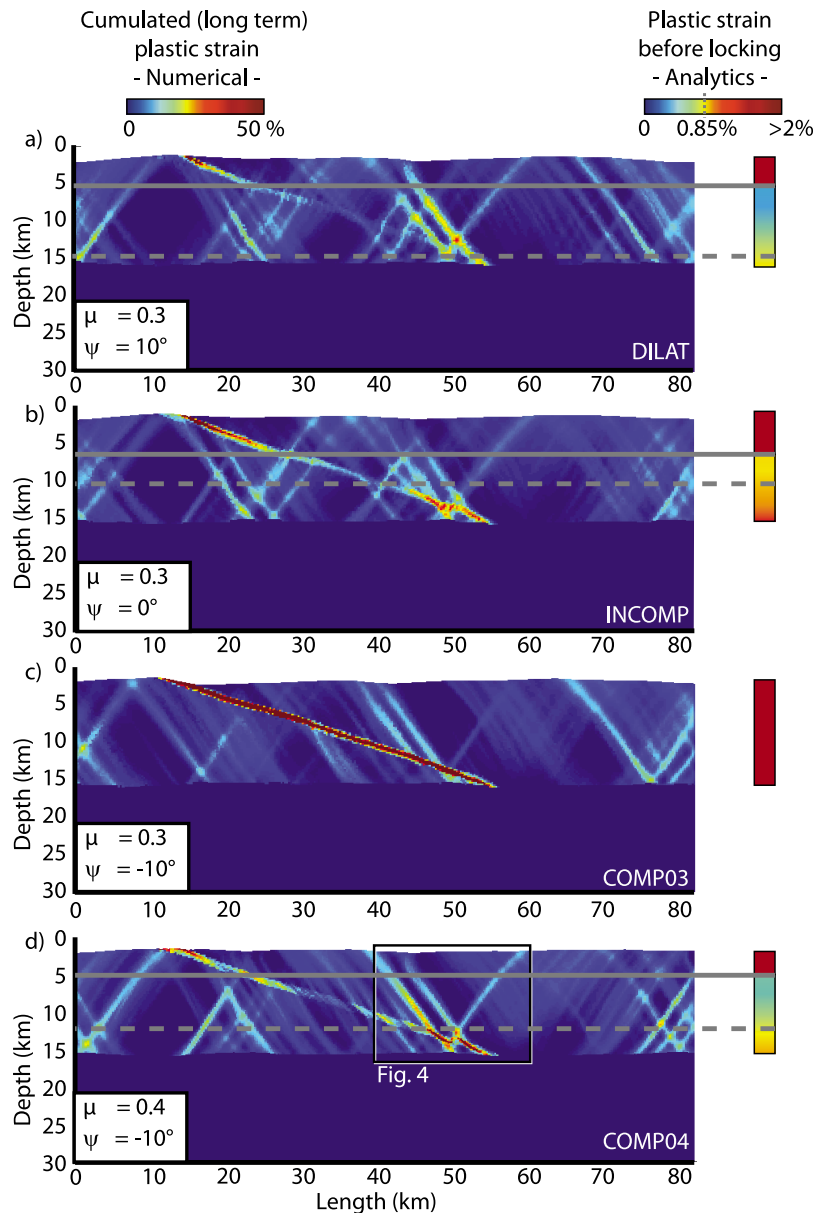
Figure 3. (a–d) Results of 2D mechanical modeling as compared to the analytical solution. Note the scale for analytic and large strain numerical models are different. The solid horizontal grey lines correspond to the predicted locking depth and the dashed horizontal grey line corresponds to plastic strain greater than 1% before locking in the analytical solution.

formation of such new secondary shear bands within the LANF, and their constant orientation is confirmed numerically at large strain on Figure 4a where secondary shear bands form with a constant dip close to 30°.

[17] For incompressible or compacting LANFs, the orientation of the secondary shear structures is consistent with the orientation of Riedel shears. Therefore, the size of newly formed structures is generally limited by the thickness of the
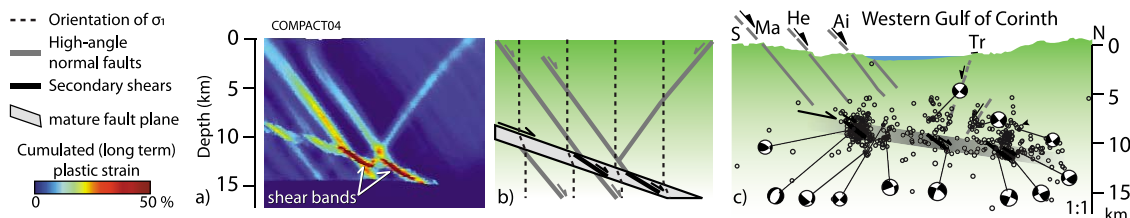
Figure 4. (a) Magnification of model COMP04, (b) sketch of the result of the model, and (c) application of the model to the distribution of Ai = Aigion fault, He = Helike fault, Ma = Mamousia fault, Tr = Trizonia Island [*Rigo et al.*, 1996].

LANF. For a 1 km-thick fault zone with a slightly negative dilation angle, these secondary shear structures are about 5 km long (Figures 4a and 4b). Assuming a square shape of the slipping patch, their surfaces reach 25 km^2. For a shear modulus of 30 GPa and an amount of slip varying from 1 mm to 10 cm, the predicted moment magnitude of an earthquake occurring on these secondary structures would correspond to Mw 2.7 to 4.7.

[18] We find that the predictions of the thick fault zone model are in agreement with observations in the western Gulf of Corinth (Figure 4). There, the cloud of micro-seismicity as reported by *Rigo et al.* [1996] is too wide (2–3 km) to be related to a single plane and the general dip of the cloud is smaller than the dips of the nodal planes. Based on our modeling results, we therefore follow the model of *Bernard et al.* [2006], in which the extension across the rift was accommodated by a creeping LANF at depth, which interacted with the high-angle normal faults bounding the rift. In this frame, we interpret the micro-seismicity in the Corinth rift as resulting from the instable slip on Riedel-type secondary shear structures newly formed within the otherwise creeping shallow-dipping fault zone. By suggesting that micro-seismicity reflects brittle shearing on structures similar to Riedel-type shears located within the LANF, the thick fault model provides a sound mechanical basis for the frequent repeated earthquakes with shallow dipping nodal planes as observed in the Gulf of Corinth [*Pacchiani*, 2006] or in the Apennines [*Chiaraluce et al.*, 2007] and more generally for the lack of large earthquakes on LANFs.

6. Conclusions

[19] When the dilation angle of a thick fault zone is smaller than its friction angle, elastic strain occurs within the fault zone to ensure the compatibility of displacement [*Lecomte et al.*, 2011]. This strain results in a rotation of principal stresses within the fault and therefore modifies the effective friction of the fault. In this paper, we demonstrate that a component of compaction of the fault zone leads to a significant drop of the effective friction of LANFs which allows faults with internal friction of 0.3 to slip at dip as low as 20°. In this regime, the thick fault model predicts that deviatoric stress rises with accumulated plastic strain on LANFs, favoring a stable slip regime. These predictions are well supported by seismological observations and geodesy in the Gulf of Corinth [*Rigo et al.*, 1996; *Bernard et al.*, 1997; *Briole et al.*, 2000; *Avallone et al.*, 2004].

[20] However, within the rotated state of stress of the fault zone, it is also possible to newly form secondary faults. These smaller faults form in a slip-weakening regime and are to that respect dynamically unstable. Their orientations depend on the dilation angle of the fault zone but in general, they are confined to the width of the fault zone and therefore their size is limited. Therefore, seismic activity on these secondary shears is necessarily of limited magnitude as it is often observed on active LANFs and other weak faults. Finally, the state of stress within the LANFs being close to steady state, the orientation of the instable secondary shear structures is constant in time, which favors the occurrence of multiplets along the shallow-dipping normal fault zone.

References

Allmendinger, R. W., K. D. Nelson, C. J. Potter, M. Barazangi, L. D. Brown, and J. E. Oliver (1987), Deep seismic reflection characteristics of the continental crust, *Geology*, 15, 304–310, doi:10.1130/0091-7613 (1987)15<304:DSRCOT>2.0.CO;2.

Avallone, A., P. Briole, A. M. Agatza-Balodimou, H. Billiris, O. Charade, C. Mitsakaki, A. Nercessian, K. Papazissi, D. Paradissis, and G. Veis (2004), Analysis of eleven years of deformation measured by GPS in the Corinth Rift Laboratory area, *C. R. Geosci.*, 336, 301–311, doi:10.1016/j.crte.2003.12.007.

Bernard, P., et al. (1997), The Ms = 6.2, June 15, 1995 Aigion earthquake (Greece): Evidence for low-angle normal faulting in the Corinth rift, *J. Seismol.*, 1, 131–150, doi:10.1023/A:1009795618839.

Bernard, P., et al. (2006), Seismicity, deformation and seismic hazard in the western rift of Corinth: New insights from the Corinth rift laboratory (CRL), *Tectonophysics*, 426, 7–30, doi:10.1016/j.tecto.2006.02.012.

Bésuelle P., J. Desrues, and S. Raynaud (2000), Experimental characterisation of the localisation phenomenon inside a Vosges sandstone in a triaxial cell, *Int. J. Rock Mech. Min. Sci.*, 37(8), 1223–1237, doi:10.1016/S1365-1609(00)00057-5.

Briole, P., A. Rigo, H. Lyon-Caen, J. C. Ruegg, K. Papazissi, C. Mitsakaki, A. Balodimou, G. Veis, D. Hatzfeld, and A. Deschamps (2000), Active deformation of the Corinth rift, Greece: Results from repeated Global Positioning System surveys between 1990 and 1995, *J. Geophys. Res.*, 105, 25,605–25,625, doi:10.1029/2000JB900148.

Byerlee, J. D., and J. C. Savage (1992), Coulomb plasticity within the fault zone, *Geophys. Res. Lett.*, 19, 2341–2344, doi:10.1029/92GL02370.

Chiaraluce, L., C. Chiarabba, C. Collettini, D. Piccinini, and M. Cocco (2007), Architecture and mechanics of an active low angle normal fault: Alto Tiberina Fault, northern Apennines, Italy, *J. Geophys. Res.*, 112, B10310, doi:10.1029/2007JB005015.

Collettini, C. (2011), The mechanical paradox of low-angle normal faults: Current understanding and open questions, *Tectonophysics*, 510, 253–268, doi:10.1016/j.tecto.2011.07.015.

Collettini, C., and R. E. Holdsworth (2004), Fault zone weakening processes along low-angle normal faults: insights from the Zuccale Fault, Isle of Elba, Italy, *J. Geol. Soc.*, 161, 1039–1051, doi:10.1144/0016-764903-179.

Collettini, C., and R. H. Sibson (2001), Normal faults, normal friction?, *Geology*, 29, 927–930, doi:10.1130/0091-7613(2001)029<0927:NFNF>2.0.CO;2.

Gerbault, M., E. B. Burov, A. N. B. Poliakov, and M. Daignières (1999), Do faults trigger folding in the lithosphere?, *Geophys. Res. Lett.*, 26, 271–274, doi:10.1029/1998GL900293.

Haines, S. H., B. A. van der Pluijm, M. J. Ikari, D. M. Saffer, and C. Marone (2009), Clay fabric intensity in natural and artificial fault gouges: Implications for brittle fault zone processes and sedimentary basin clay fabric evolution, *J. Geophys. Res.*, 114, B05406, doi:10.1029/2008JB005866.

Hayman, N. W., J. R. Knott, D. S. Cowan, E. Nemser, and A. Sarna-Wojcicki (2003), Quaternary low-angle slip on detachment faults in Death Valley, *Calif. Geol.*, 31, 343–346.

Ikari, M. J., A. R. Niemeijer, and C. Marone (2011), The role of fault zone fabric and lithification state on frictional strength, constitutive behavior, and deformation microstructure, *J. Geophys. Res.*, 116, B08404, doi:10.1029/2011JB008264.

Jackson, J. A., and N. J. White (1989), Normal faulting in the upper continental crust: Observations from regions of active extension, *J. Struct. Geol.*, 11, 15–36, doi:10.1016/0191-8141(89)90033-3.

Lecomte, E., L. Jolivet, O. Lacombe, Y. Denèle, L. Labrousse, and L. Le Pourhiet (2010), Geometry and kinematics of Mykonos detachment (Cyclades, Greece): evidence for slip at shallow dip, *Tectonics*, 29, TC5012, doi:10.1029/2009TC002564.

Lecomte, E., L. Le Pourhiet, O. Lacombe, and L. Jolivet (2011), A continuum mechanics approach to quantify brittle strain on weak faults: Application to the extensional reactivation of shallow dipping discontinuities, *Geophys. J. Int.*, 184, 1–11, doi:10.1111/j.1365-246X.2010.04821.x.

Lister, G. S., and G. A. Davis (1989), The origin of metamorphic core complexes and detachment faults formed during Tertiary continental extension in the northern Colorado River region, U.S.A., *J. Struct. Geol.*, 11, 65–94, doi:10.1016/0191-8141(89)90036-9.

Mair, K., S. Elphick, and I. Main (2002), Influence of confining pressure on the mechanical and structural evolution of laboratory deformation bands, *Geophys. Res. Lett.*, 29(10), 1410, doi:10.1029/2001GL013964.

Makris, J., and R. Vees (1977), Crustal structure of the central Aegean Sea and the islands of Evia and Crete, Greece, obtained by refractional seismic experiments, *J. Geophys. Res.*, 42, 329–341.

Mehl, C., L. Jolivet, and O. Lacombe (2005), From ductile to brittle: Evolution and localization of deformation below a crustal detachment (Tinos, Cyclades, Greece), *Tectonics*, *24*, TC4017, doi:10.1029/2004TC001767.

Mehl, C., L. Jolivet, O. Lacombe, L. Labrousse, and G. Rimmele (2007), Structural evolution of Andros Island (Cyclades, Greece): A key to the behaviour of a (flat) detachment within an extending continental crust, in *The Geodynamics of the Aegean and Anatolia*, edited by T. Taymaz, Y. Dilek, and Y. Yžlmaz, *Geol. Soc. Spec. Publ.*, *291*, 41–73, doi:10.1144/SP291.3

Niemeijer, A., D. Elsworth, and C. Marone (2009), Significant effect of grain size distribution on compaction rates in granular aggregates, *Earth Planet. Sci. Lett.*, *284*, 386–391, doi:10.1016/j.epsl.2009.04.041.

Numelin, T., C. Marone, and E. Kirby (2007), Frictional properties of natural fault gouge from a low-angle normal fault, Panamint Valley, California, *Tectonics*, *26*, TC2004, doi:10.1029/2005TC001916.

Pacchiani, F. (2006), Etude sismologique des failles normales actives du rift de Corinthe, PhD thesis, Univ. Paris XI, Paris.

Platt, J. P., and R. L. M. Vissers (1980), Extensional structures in anisotropic rock, *J. Struct. Geol.*, *2*(4), 397–410, doi:10.1016/0191-8141(80)90002-4.

Poliakov, A. N. B., Y. Podladchikov, and C. Talbot (1993), Initiation of salt diapirs with frictional overburdens: Numerical experiments, *Tectonophysics*, *228*, 199–210, doi:10.1016/0040-1951(93)90341-G.

Rigo, A., H. Lyon-Caen, R. Armijo, A. Deschamp, D. Hatzfeld, K. Makropoulos, P. Papadimitriou, and I. Kassaras (1996), A microseismicity study in the western part of the Gulf of Corinth (Greece): Implications for large-scale normal faulting mechanisms, *Geophys. J. Int.*, *126*, 663–688, doi:10.1111/j.1365-246X.1996.tb04697.x.

Roscoe, K. H., A. N. Schofield, and C. P. Wroth (1958), On the yielding of soils, *Geotechnique*, *8*, 22–53, doi:10.1680/geot.1958.8.1.22.

Sagy, A., and E. E. Brodsky (2009), Geometric and rheological asperities in an exposed fault zone, *J. Geophys. Res.*, *114*, B02301, doi:10.1029/2008JB005701.

Sibson, R. H. (1990), Rupture nucleation on unfavourably oriented faults, *Bull. Seismol. Soc. Am.*, *80*, 1580–1604.

Tirel, C., J. P. Brun, and E. Burov (2004), Thermo-mechanical modeling of extensional gneiss domes, in *Gneiss Domes in Orogeny*, edited by D. L. Whitney, C. Teyssier, and C. S. Siddoway, *Spec. Publ. Geol. Soc. Am.*, *380*, 67–78.

Vermeer, P. (1990), The orientation of shear bands in biaxial tests, *Geotechnique*, *40*, 223–236, doi:10.1680/geot.1990.40.2.223.

Yamato, P., P. Agard, E. Burov, L. Le Pourhiet, L. Jolivet, and C. Tiberi (2007), Burial and exhumation in a subduction wedge: Mutual constraints from thermomechanical modeling and natural P-T-t data (Schistes Lustrés, western Alps), *J. Geophys. Res.*, *112*, B07410, doi:10.1029/2006JB004441.

E. Lecomte, Institute of Petroleum Engineering, Heriot-Watt University, Edinburgh EH14 4AS, UK. (emmanuel.lecomte@pet.hw.ac.uk)

O. Lacombe and L. Le Pourhiet, ISTEP, UMR 7193, UPMC, Université Paris 6, F-75005, Paris, France.